Particle size distribution (PSD) estimation using unmanned aerial vehicle (UAV) photogrammetry for rockfill shear strength characterization

Marco Arrieta[1] (iD) · Zong-Xian Zhang[1]

Abstract

The strength of rockfills and waste materials is significantly influenced by their particle size distribution (PSD). For large waste rockfills, PSD is fundamental to determine the shear behavior. Traditionally, PSD for rockfill, used in materials like coarse-grained aggregates, has been obtained through physical sieving. However, the particle sizes in hard rockfills can vary significantly from small particles (< 20 cm diameter) to large blocks or boulders over 100 cm, with the maximum size limited by the in situ ground conditions and blasting performance. Essentially, the sieving process is impractical, considering the scale of the mine waste dumps and the time required. Therefore, in this study, a workflow using digital detection to estimate the PSD is presented, aiming to quantify the waste dump shear strength using Barton–Kjaernsli empirical criterion. PSD from UAV is validated using manual field measurements of individual boulders. The error for coarse characteristic size prediction ranges within ± 4 mm, and the increase in the data collection frequency, area covered, and resolution of fragmentation measurement for rockfills and waste dumps using UAV allows to improve the statistical reliability of the PSD and fragmentation measurement.

1 Introduction

Blasted and crushed waste rocks from surface and underground mines are commonly deposited in waste dumps and stockpiles. Finer waste materials, further refined during mineral processing, are stored in Tailing Storage Facilities (TSF) [44]. To effectively manage these mining by-products, thorough geotechnical characterization is necessary to anticipate future ground behavior and risk. A key aspect of this is determining the mechanical properties, particularly shear strength, of rockfills in waste dumps. Rockfill, frequently used in structures such as embankment dams, retaining walls, shoring systems, and ground improvements, consists of rock fragments varying in size from

gravels (+ 2 mm), cobbles (+ 60 mm), and boulders (+ 200 mm), with the largest fragments reaching 1000 mm.

Particle size distribution (PSD) and shape characteristics are key in geotechnical design and construction of rockfill and waste dumps. These factors directly affect the strength and load-bearing capacity of granular materials [109] and have significant economic implications for construction projects. PSD role in rockfill structures is multifaceted [90]. It influences rockfill compaction and must meet specific design acceptance criteria for construction quality control [76]. The design of rockfill dams and waste piles necessitates knowledge of in situ material properties, including deformation, permeability, shape, and shearing strength [52]. Nonlinear shear strength behavior for waste dumps and rockfill correlates PSD and confinement stress with shear strength and deformability [17, 49, 57, 63]. Well-graded material demonstrates enhanced densities and shear strength, a result of increased inter-granular contact [28]. Empirical evidence indicates a decrease in the

✉ Marco Arrieta
    Marco.ArrietaRodriguez@student.oulu.fi

[1] Oulu Mining School, University of Oulu, 90014 Oulu, Finland

intrinsic strength of larger particles in rockfills [34, 65, 69, 70], highlighting the vital correlation between PSD and the shear strength of rockfills and waste dumps [41].

Investigating the physical and mechanical properties of rockfill material is critical for the construction of waste dumps and rockfill dams. However, triaxial testing on prototype rockfill using conventional laboratory equipment is often impractical due to the large size of field aggregates [106]. This necessitates the development of appropriate methods for determining PSD at a realistic scale [63].

Conventionally, engineering materials PSD is assessed through physical sieve analysis employing screens with squared mesh [20]. Rockfill materials PSD is typically established via visual rock gradation analysis, reliant on visual examination and engineer expertise for construction quality control [53]. This method, involving sieving finer fractions (i.e., up to 60 mm) and measuring larger rocks, is expensive, time consuming, and not feasible for routine quality control [87].

Full-scale gradation tests on rockfill and waste dump samples demand significant field work, often requiring up to 48 h [64]. These tests are generally conducted by a field geotechnical engineer and an assistant [77] and need machinery and safe handling for larger particles (i.e., heavier particles) [47]. Therefore, it is imperative to develop a more efficient, safer, and simpler method for routine assessment of rockfill material size distribution, leveraging the latest advancements in computer science and technology [58].

Small-scale mechanical testing for coarse materials often involves adjusting the PSD, specifically reducing the maximum grain size to fit samples within laboratory devices [76]. This approach presumes that the adjusted PSD is comparable to the original grading in stress–strain behavior. However, changes in particle size may alter individual grain properties, including shape and crushing strength [25]. Although parallel scaling is a common technique in rockfill materials [39], the effects of particle size correlations are not often considered, and their impacts are not thoroughly understood [29].

Scaling-down techniques yield a modified gradation compared to the original field material. Contrary to popular belief, employing parallel scaling-down methods also alters the physical composition. As a result, both scalping and parallel techniques can predict the shear strength of field rockfill by extrapolating laboratory shear test results when normal stress is high. However, these techniques are ineffective for low to intermediate normal stress [37]. Inverse correlations between particle size and strength can lead to decreased particle crushing in finer samples, while size–shape correlations might cause increased crushing in finer samples comprised of more elongated grains [35]; vertical

and lateral segregation can result in overestimation or underestimation of the final shear strength; this is due to significant lateral heterogeneity, which causes considerable variations in the geotechnical properties of waste rock in practical scenarios [83]. It follows, by analogy, that friction angles of field samples, when evaluated using the scalping scaling-down technique, can be accurately predicted. In contrast, predictions based on the parallel scaling-down technique may be deemed unreliable for active mines or real-case scenarios [36].

Recent developments in image processing technology present new opportunities for determining the PSD of rockfill and waste dump materials [105]. Similar to traditional visual assessments, this method uses computer algorithms to inspect and measure visible particles in digital photographs [56]. This approach enhances the efficiency of geotechnical characterization for rockfills and waste dumps by reducing data collection time and increasing time for engineering analysis [60]. The integration of UAV technology with advanced image processing marks a significant shift, enabling aerial photogrammetry for PSD estimation, a technique previously used in topographical surveys and geological mapping and is now a viable alternative to conventional sieve analysis [93].

Based on the established background, this study employs UAV technology and advancements in computer image processing for PSD determination in aerial photogrammetry, focusing on waste dumps and rockfill shear strength characterization. The integration of UAV technology has enabled increases in measurement frequency, area coverage, and resolution in fragmentation measurements for rockfills and waste dumps. This method has improved the statistical reliability of both PSD and fragmentation measurements, enhancing the precision of geotechnical characterization methods.

2 Material and methods

2.1 Previous shear strengths for granular materials—rockfills and waste dumps.

The shear strength of granular materials, including rockfills and mine waste dumps, quantifies the resistance manifested when particles are induced to move in the shear direction under a specified normal load. This resistance, often referred to as friction, is notably influenced by particle size, shape, intrinsic strength, and surface roughness [98]. Newland and Allely [72] employed a nonlinear function to characterize the shear strength of granular materials. Under a specific normal stress, the shear stress is influenced by both the angle of frictional sliding resistance between

particles and the mean deviation angle of particle displacements from the applied shear direction.

De Mello [67] presented an empirical power curve envelope ideally suited for characterizing the strength envelope of rockfill materials in dam embankments. Charles and Watts [28] adopted the power law envelope for shear strength representation. Barton–Kjaernsli [74] devised a shear strength criterion for rockfills, drawing inspiration from the empirical joint shear criterion proposed by Barton in 1973. Gonzalez [45] derived a logarithmic strength envelope based on published findings from large-scale triaxial and direct shear box tests.

Sarac and Popovic [89] conducted an extensive analysis of numerous large-scale direct shear tests executed at the Institute for Geotechnics and Foundation Engineering. The tested materials primarily comprised limestone, sandstone, serpentinite, and slate, sourced from a combination of natural rock debris and quarry rockfill. Testing was predominantly conducted on materials intended for embankment dams, with stress ranges spanning from 0.05 to 2.0 MPa.

Charles [27] determined that the shear strength of densely compacted rockfill is markedly influenced by both placement density and stress level. A simple power regression, $\tau_f = A\sigma_n^b$, generally provides an accurate representation of the failure envelope. The parameters A and B can be derived from a series of drained triaxial compression tests conducted on the compacted rockfill under suitable confining pressures. Doruk [40], utilizing both published data and data from fractured rocks, modified the original Hoek and Brown criteria for rockfill materials by setting the rockfill compressive strength to zero (S = 0). Indraratna [48, 50] formulated a nonlinear equation of $\tau_f = A\sigma_n^b$ applicable to both shear stress and principal stress under both static and dynamic triaxial loading conditions. The findings underscored that while shear strength and particle degradation (breakage) are influenced by the materials particle size distribution, they are primarily affected by the imposed confining pressure. Additionally, employing large-scale triaxial equipment, Indraratna generated specific geotechnical data on the shear strength and the angle of internal friction of ballast relative to particle size distribution. This led to the development of a nonlinear relationship elucidating the fluctuations in shear strength, angle of internal friction, dilation rate, and extent of particle crushing at varied confining pressures and principal stress ratios [49].

Xu [103] proposed a methodology to estimate the shear strength of rockfills and granular materials using the fractal model for particle crushing. Nonetheless, the derived outcomes often diverged from experimental findings, primarily due to the challenges in procuring the PSD and estimating the fractal dimension. In subsequent research, Xu [102] introduced a shear strength function anchored in the fractal model for particle fragmentation. This model advocates a power law function as the optimal representation for the shear strength criterion of granular materials. Experimental data from municipal solid waste incineration confirmed the model validity.

In addressing the complexity of shear strength in rockfills and waste dumps, Table 1 plays a critical role. This table provides an overview of the previously studied shear strengths of granular materials and their respective mathematical formulations. Among the 11 previous shear strength criteria reviewed, it is evident that 10 of these are not adequately suited for large-scale applications, primarily due to limitations in their methodologies or the scope of their validation. For instance, De Mello [67], Charles, and Watts [28], who presented the current power law for general applications. However, the A and B parameters in their formula are not truly general and require extensive site-specific data for accurate definition, thus posing limitations for broader applications. Sarac and Popovic [89] methodology fails to consider the nonlinear relationship between normal stress and uniaxial compressive stress, leading to inaccuracies in their formulation, especially in unit consistency.

Similarly, Gonzalez [45] approach necessitates a large amount of triaxial data, which is often impractical for real-case scenarios. Charles [27] method presents another challenge in the estimation of constants $C1$ and $C2$, as it requires a substantial volume of triaxial results for site-specific accuracy. Xu [103] methodology, while based on the fractal model for particle crushing, often resulted in outcomes that diverged from experimental findings, underscoring the challenges in procuring the particle size distribution and accurately estimating the fractal dimension.

Utilizing the criteria from Table 1 and acknowledging the Barton–Kjaernsli criterion effectiveness, this study combines it with UAV technology for precise PSD estimation. This fusion targets shear strength characterization in large-scale rockfills and waste dumps. By aligning UAV photogrammetry with this established empirical approach, the study aims to enhance the accuracy and applicability of geotechnical analysis in these crucial areas, offering a balanced blend of technological innovation and proven methodology.

2.2 Shear Strength model for rockfill, stockpiles, and mine waste dumps—Barton–Kjaernsli criterion.

Estimating shear strength in coarse materials, with particle sizes ranging from a few to several dozen centimeters, poses a challenge due to the limitations of commercial

Table 1 List of shear strengths for granular materials and their mathematical form

Author/failure criterion	Mathematical form	Parameters	Remarks	References
Newland and Allely, 1957	$\tau = \sigma_n\prime(\varphi_b\prime + i)$	σ_n: Normal stress	Empirical curved envelope	[72]
		φ_b: Basic friction angle	Following the principle for discontinuities	
		i: Average deviation angle of particle		
De Mello, 1977	$\tau = A\sigma_n^B$	A, B: Fitting parameters	Empirical curved envelope	[28, 67]
Charles and Watts, 1980		σ_n: Normal stress	Laboratory test required to calibrate A and B	
Barton and Kjaernsli, 1981	$\varphi\prime = R\log\left(\frac{S}{\sigma_n}\right) + \varphi_b$	R: Equivalent roughness	Extension Barton, 1973	[74]
		S: Equivalent particle strength	Parameters based on trial-and-error fitting on triaxial data, Leps, 1973	
		σ_n: Normal stress	Applicable at large scale with limitations	
		φ_b: Basic friction angle		
Sarac and Popovic, 1985	$\tau_{max} = A\left(\frac{\sigma_n}{\sigma_0}\right)^B$	A, increases when $\sigma_c \uparrow C_u \uparrow \gamma \uparrow d_{50} \uparrow$, 0.7 to 1.5	Developed from large-scale direct shear tests (up to σ_n = 2 MPa) on rockfill and gravels	[89]
		B, increases when $\sigma_c \uparrow C_u \uparrow \gamma \downarrow$, 0.419 to 0.911		
Gonzalez, 1985	$\varphi\prime = \varphi_0 - j\log_{10}\left(\frac{\sigma_{nf}}{\sigma_{c0}}\right)$	j,: Constant for specific materials and conditions	Logarithmic based on published results	[45]
		σ_{nf}: Normal stress	Required large amount of triaxial data	
		σ_{c0}: Unconfined Strength		
Charles, 1991	$\varphi\prime = C_1\log\left(\frac{C_2}{\sigma_3\prime}\right) + \varphi_b\prime$	φ_b: Basic friction angle	Similar approach, Barton and Kjaernsli, 1981	[27]
		C_1, C_2: Constants		
Doruk, 1991	$\sigma_1\prime = \sigma_3\prime + \left(\frac{m\sigma_3\prime}{\sigma_c}\right)^a \sigma_c$	m, a: Hoek and Brown parameters	Developed from Hoek and Brown	[40]
Indraratna, et al., 1993	$\frac{\sigma_1\prime}{\sigma_c} = \alpha\left(\frac{\sigma_3\prime}{\sigma_c}\right)^\beta$	α, β: 0.4, 0.62 (lower bound, 0.1 to 1 MPa)	Alternative for principal stresses	[48, 50]
Indraratna, 1994		α, β: 0.78, 0.65 (upper bound, 0.1 to 1 MPa)		
		α, β: 2.71, 0.96 (lower bound, 1 to 7 MPa)		
		α, β: 3.58, 0.90 (upper bound, 1 to 7 MPa)		
Indraratna, et al., 1998	$\frac{\sigma_1\prime}{\sigma_3\prime} = a\sigma_3\prime^b$	a, b: 84.98–0.49 (gradation A)	Developed empirically for two gradations	[49]
		a, b: 125.17–0.56 (gradation B)	Non-convergence $\sigma_n = 0$, low stress	
Xu, et al., 2015	$\tau_f = a\sigma_n^b$	$a = k^{\frac{D}{3}}l^{\frac{(6-2D)}{3}}$	Based on fractal fragmentation–D	[103]
		$b = \frac{D}{3}$	k: Constant	
Xu, 2018	$\tau_f = a\sigma_n^b$	$b = \frac{2(2D-3)}{3(D-1)}$	Based on fractal fragmentation–D	[102]
			"a" parameter estimation is not clear	

laboratory testing devices. These devices are typically designed for samples with particles up to a centimeter [16]. Consequently, shear strength estimation often relies on the empirical model by Nick Barton and Bjorn Kjaernsli (1981) [74], known as the B–K criterion. This model accounts for the nonlinearity of the shear strength envelope, particularly in coarse granular materials under high loads [78]. The B–K criterion parameterizes shear strength using equivalent roughness (R) and equivalent strength (S) [14].

The B–K empirical model, presented as Eq. (1), defines τ as the shear strength. This nonlinear model is particularly suited for characterizing coarse materials such as rockfill and blasted rocks, known for their nonlinear shear strength envelope [17]. Within this model, the effective friction angle of waste rock is determined by the roundness of the particles and the porosity of their arrangement [97]. The friction angle, at minimum, equals the basic friction angle, varying by a magnitude R for a tenfold increase in the ratio of $\frac{S}{\sigma_c}$ [15].

$$\tau = \sigma_n \tan \left[R \, \mathrm{Log}_{10}(S/\sigma_n) + \varphi_b \right] \qquad (1)$$

where

σ_n = Effective normal stress.

φ_b = Basic friction angle of waste (dump) particles.

R = Equivalent roughness of waste (dump) particles.

S = Size-dependent equivalent strength of waste (dump) particles.

σ_c = Uniaxial compressive strength of the intact rock.

In the Barton–Kjaernsli model, the parameter R is linked to the roundness and porosity (n) of particle arrangements, determined from Barton–Kjaernsli chart. R values range from 0 to 15, representing loose arrangements of rounded, smooth particles to dense arrangements of very angular and rough particles. The S parameter depends on the uniaxial compressive strength (σ_c or UCS) of the rock and its characteristic particle size, denoted as PSD (D_{50}). D_{50} refers to the median particle diameter in the cumulative distribution, indicating that 50% of particles are larger and 50% smaller than this size. D_{50} is typically used to represent a group of particles size [14].

2.3 UAV photogrammetry in particle size distribution analysis

Research on particle size measurement using machine vision has been active since the 1980s [5, 75]. Gallagher [43] introduced an early image processing system for analyzing the size distribution of fragmented particles on conveyor belts, using a chord sizing method for edge delineation. Nyberg [104] developed a similar system, scanning chord sizes on edges of fragmented rock images in muck-piles, furthering the application of this technology.

Feng [62] described a method for segmenting ore images into regions to estimate fragment size distributions. Wu and Kemeny [100] developed an automated system for sizing rock fragments post-blasting. Lin [59] employed edge detection algorithms to identify particles and estimate sieve size distributions using measured chord lengths.

Koizumi [54] in 1994 addressed the issue of partially obscured particles, fitting circular approximations to two-dimensional projections of particle edges. Yen [107] developed a watershed segmentation algorithm, although results were not completely satisfactory, even with well-sorted particles and good backgrounds.

Since 2000, image processing for fragmented rock particles has gained significant research interest, with various algorithms developed for measuring rock fragment sizes in applications like gravitational flows, conveyors, muck-piles, and laboratories [104]. Casali [26] implemented machine vision and image segmentation for ore sorting and particle size distribution in mining processing. Matthew [94] offered a mathematical and image analysis method to determine rock pile size distribution, focusing on surface size class proportions. Bujak and Bottlinger [22] designed a system for three-dimensional particle shape measurement using free-fall analysis, capturing particles from three orthogonal directions for 3D reconstruction.

In 2009, Thurley [95] introduced an automated system for measuring limestone fragment size distribution on conveyor belts using 3D range data. This technology aimed to enable automatic control of particle breaking or aggregation processes, enhancing energy efficiency and product quality. Sanchidrian [88] evaluated the performance of image analysis on photographed materials, comparing it to sieve-obtained size distributions. He also investigated the efficacy of various functions in fitting the data and extrapolating toward finer particle sizes.

In 2012, Zhang [110] estimated the particle size distribution of overlapped coal particles using image segmentation. This process involved image enhancement algorithms to distinguish overlapped particles by darkening material in lower layers. Subsequently, in 2014, Hamzeloo [46] employed image processing and neural network techniques to determine the particle size distribution in a copper concentrator crushing circuit.

In 2016, a study [6] introduced laboratory-scale rock fragment measurements using a quadrotor UAV with a camera, highlighting aerial fragmentation analysis' prediction accuracy and time efficiency. Bamford in 2017 [7] investigated UAVs with artificial lighting for measuring rock fragmentation in poor lighting, typical of night shifts in surface mines or underground mines. This research conducted both indoor and outdoor experiments using a quadrotor UAV for rock fragmentation analysis.

In 2018, Cardona [24] introduced a framework for processing images from inline imaging probes, adding a focus evaluation to exclude out-of-focus particles and extract accurate shape and size data. Stauder in 2018 [92] estimated PSD by combining 3D surface and 2D image analysis, aiming to reduce manual post-processing and user interaction. Jang in 2019 [51] presented a 3D rock fragmentation measurement system (3DFM) overcoming the limitations of traditional 2D photograph-based methods, validated through laboratory comparisons with 100 randomly collected rock fragments.

In early 2020, Bamford [9] demonstrated the use of UAV systems for monitoring and improving blasting processes in open-pit mines, focusing on post-blast analysis of rock piles for fragmentation assessment. In 2021, Bamford [8] had progressed to evaluating rock fragmentation measurement using deep learning, employing a deep neural network to predict rock fragment sizes from 2D images. In 2022, Abderrazak [86] applied the Kuz–Ram empirical model and digital image processing, utilizing softwares like

WipFrag and Split-Desktop, for analyzing particle size distribution in a limestone quarry.

In this study, the limitations of existing PSD estimation methods and 2D image processing software, including IPACS, TUCIPS, and GoldSize, are addressed. These conventional approaches, while popular, require object scaling, are time consuming for manually splitting fine fragments, and are mainly effective on a smaller scale. They have not been used for full-scale rockfill and waste dump analysis, nor for estimating shear strength. To overcome these challenges, UAV technology was used to acquire high-resolution (effective pixels: 12 M) [55] images of multiple waste dumps. These images were analyzed with Fragmenter from 3GSM [42], and a field survey measuring 50 rock boulders validated the image-derived particle sizes, ensuring accurate PSD and shear strength estimation (Fig. 1).

The workflow outlined in Fig. 2 includes four steps: (1) reconstructing a 3D model using UAV digital photogrammetry, (2) selecting and discretizing the area for analysis, (3) automatically characterizing the PSD, and (4) producing PSD plots and conducting a grain size analysis.

Figure 2 is structured to estimate the D_{50} of waste dump particles, essential for calculating their size-dependent equivalent strength (S). This methodology is critical for a comprehensive analysis of particle behavior in waste dumps, ensuring a precise and thorough assessment of particle size distribution (PSD).

3 Results and discussion

3.1 Geography and climate overview of the site.

Waste dump materials for this study were sourced from an open-pit project in the Caribbean archipelago, situated at an altitude between 300 and 500 m above sea level. The mine experiences a tropical climate, with average annual rainfall ranging from 1843 to 1956 mm. Rainfall is year-round, with the wet season (May to November) seeing nearly double the precipitation of the drier months, often in the form of intense tropical storms [12].

3.2 Geological and geomorphological setting of the site.

In the mine district, gold mineralization is associated with early Cretaceous volcanic domes [30]. Since mining started in 1975, two main deposits and several smaller ones have been sources of ore [71]. The near-surface materials in this region are often highly weathered and saprolitic. The Caribbean commonly features thick saprolite sequences or residual soils, reaching up to 20 m [96]. The geological formation comprises a lower complex with various volcanic features and is overlain by volcaniclastic sedimentary rocks, representing a lower Cretaceous intra-oceanic setting [18].

The Hatillo Thrust Fault (HTF) in the region dips approximately 30° southwest, with directions ranging from 200° to 225°, and runs parallel to the Cordillera Central axis [66].

The volcanoclastic sedimentary unit has experienced significant seawater metamorphism, leading to spilitization. This has resulted in lithologies being identified as spilite and keratophyre [66]. Notably, in the Seibo tectonic terrane, Albian carbonate deposition overlays the volcanoclastic formation unconformably, evident in the central and eastern parts of the site [82].

3.3 Characteristics of waste dump materials.

This study investigates five waste dumps, both blasted and quarried. The characteristics of these waste dump materials are outlined in Table 2, and the gradation curves for the rockfill are presented in Fig. 3. The intact rock uniaxial compressive strength ranges from 14 MPa (WD-1) to
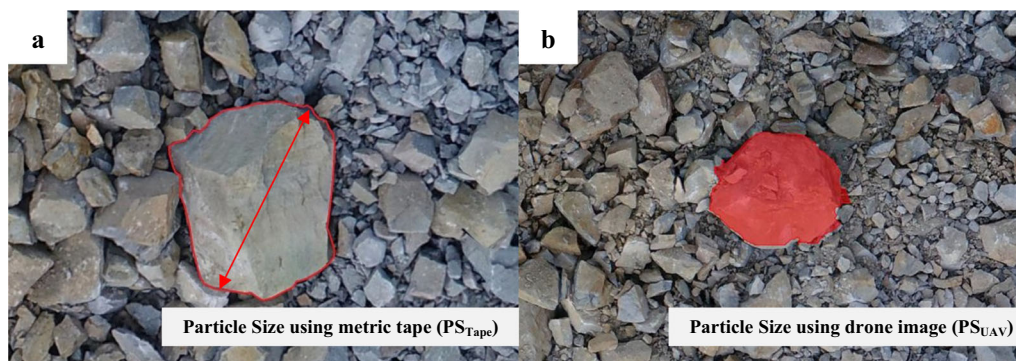

Fig. 1 Particle size measurements using manual and image processing. **a** Manual measurements using metric tape for particle size. **b** Particle size measurements using image processing
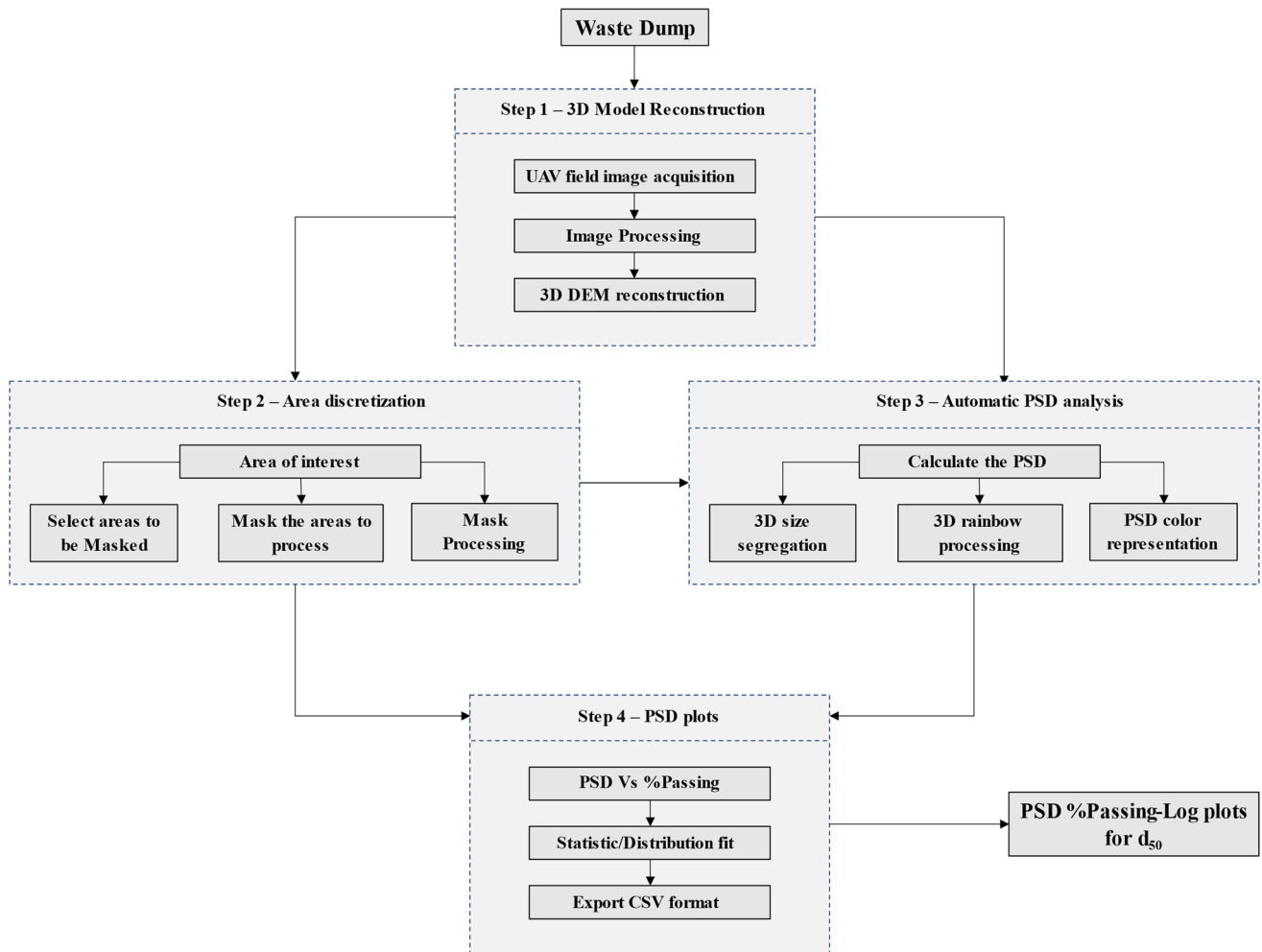
Fig. 2 Workflow for PSD using UAV photogrammetry

Table 2 Properties of waste dump materials

Site	Uniaxial compressive strength σ_c (MPa), intact rock	Density ρ (g/cm^3), intact rock	D10 (mm)	D30 (mm)	D50 (mm)	D60 (mm)	Cu	Cc
WD-1	14	2.65	8.5	83.1	199.7	267.4	31.6	3.1
WD-2	30	2.80	37.4	77.2	135.3	165.0	4.4	1.0
WD-3	18	2.77	3.2	48.8	109.2	151.8	47.9	5.0
WD-4	35	2.79	186.6	468.5	787.6	845.4	4.5	1.4
WD-5	40	2.80	47.7	121.6	248.3	310.3	6.5	1.0

40 MPa (WD-5), informed by long-term testing at the mine site. The five waste dumps (Fig. 4) described in the study are characterized as follows:

- WD-1: Characterized by a high potential for acid generation and significant sulfide content, this carbonaceous-sediment mudstone exhibits a uniaxial compressive strength of 14 MPa. Particle sizes in this mudstone have been observed to reach as large as 2155 mm.

- WD-2: In tropical conditions, the limestone exhibits low to medium physical alteration. Its geological fabric influences the maximum particle size, observed post-dumping to be 622 mm. Composed predominantly of gravel and sand, the brittle nature of the limestone and its jointed or blocky geological structure are significant. It possesses a geological stress index (GSI) of 70.

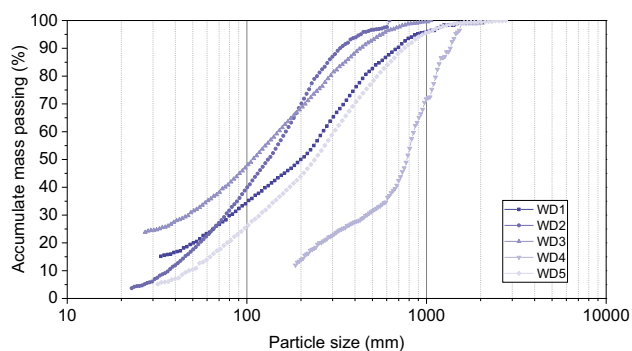- WD-3: Notable for its high potential acid generation (PAG) capacity and rich sulfide content, this

Fig. 3 Comparative particle size distribution across the five waste dumps

carbonaceous-sediment mudstone is also marked by laminar mineralization associated with micaceous minerals. The mudstone uniaxial compressive strength is 18 MPa, with particle sizes documented up to 1057 mm.

- WD-4 and WD-5: Comprising volcanoclastic and PAG materials, these samples are distinguished by their coarse, rocky nature, and a low proportion of fines. Particle sizes for WD-4 have been measured up to 1978 mm and for WD-5 up to 2761 mm. The intact

rock, andesite, shows a uniaxial compressive strength ranging from 35 to 40 MPa, classified from brittle to semi-brittle, with noticeable faults and joints. The GSI stands at 60.

3.4 Techniques for 3D model reconstruction using UAV imagery.

The red/green/blue (RGB) images captured by an unmanned aerial vehicle (UAV) serve as the input for reconstructing a 3D model in the form of a point cloud. This is achieved using the Structure-from-Motion (SfM) technique, a form of photogrammetry that employs computer algorithms to identify key points in overlapping images taken from multiple angles, facilitating the creation of 3D models [99]. By applying a mask to the area of interest, as outlined in Fig. 2, vegetation is effectively filtered out from the point cloud [1].

SfM (Structure-from-Motion) processing reconstructs a three-dimensional structure of a stationary scene from a collection of two-dimensional images captured from various positions and angles. This technique involves motion estimation of the camera corresponding to each image [80].
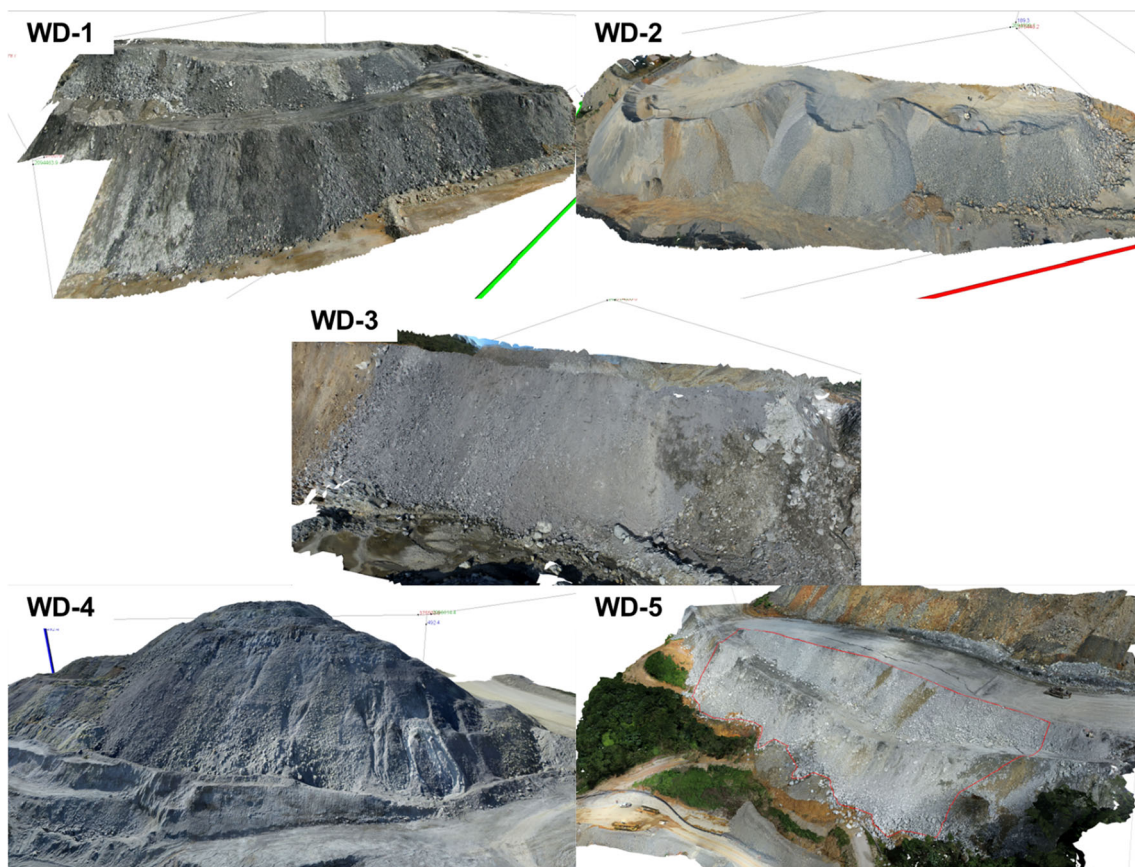

Fig. 4 3D views from UAV photogrammetry of the five waste dumps

A variety of software packages for generating 3D point cloud models are currently available. For the purpose of this study, Fragmenter (accessible at https://3gsm.at/produkte/bmx-fragmenter/) was employed, in accordance with the workflow showed in Fig. 2.

For image acquisition in the field, a DJI Mavic Pro quadrotor drone was utilized. This quadcopter platform is equipped with a 1/2.3″ CMOS sensor, boasting 12.35 million effective pixels (total pixels: 12.71 million), suitable for photogrammetric surveys [108]. The UAV system, featuring a remote flight controller, establishes a wireless connection to a DJI controller or a cellphone. Details regarding the UAV system and the on-board camera are presented in Table 3. The primary field activities comprised three stages: (1) designing the flight mission, (2) placing and acquiring ground control points (GCPs), and (3) conducting flight operations and collecting aerial images.

3.5 Particle size validation: Comparing digital analysis with field measurements.

In order to validate the digital measurements, manual assessments of rock boulder diameters were conducted across all five waste dumps. During the field investigation, boulder locations were marked to ensure they were fully captured in the drone photographs. For the validation of the digital particle size distribution (PSD) results, a sample comprising 50 boulders (10 per waste dump, as indicated in Table 4 and illustrated in Fig. 5) was used. To improve their visibility during image processing, boulders and fragments that could be captured in the UAV photographs were painted blue and positioned in the crest area of the waste dumps.

For each waste dump, the comparison between manually measured and digitally determined particle sizes revealed the following results:

- WD-1: Average deviation of 12.3 mm and standard deviation of 16.9 mm, with a mean difference of 14 mm.

Table 4 Comparison of results between digital analysis and field measurements for particle size

Site	Method	Number of datasets	Mean value (mm)	Std.	Error (%)
WD-1	Field	10	232	16.9	6.9
	UAV		218	12.3	
WD-2	Field	10	241	43.3	5.3
	UAV		240	42.4	
WD-3	Field	10	205	21.7	5.7
	UAV		199	14.2	
WD-4	Field	10	217	49.9	4.4
	UAV		220	52.5	
WD-5	Field	10	248	41.0	4.7
	UAV		242	39.1	

- WD-2: Average deviation of 43.3 mm and standard deviation of 42.4 mm, with a mean difference of 1 mm.
- WD-3: Average deviation of 21.7 mm and standard deviation of 14.2 mm, with a mean difference of 6 mm.
- WD-4: Average deviation of 49.9 mm and standard deviation of 52.5 mm, with a mean difference of 3 mm.
- WD-5: Average deviation of 41.0 mm and standard deviation of 39.1 mm, with a mean difference of 6 mm.

To assess the errors in field particle size between digital analysis and manual measurements, a deviation ratio or error (DR, as per Eq. 2) was calculated. The average DR values across the five case studies were 6.9, 5.3, 5.7, 4.4, and 4.7%, respectively (refer to Fig. 6).

The deviation ratio (DR) is calculated using the formula

$$DR = \Delta|PS|/PS_{Tape} \qquad (2)$$

In this equation, $\Delta|PS|$ represents the difference in particle size as determined by digital analysis (PS_{UAV}) and manual measurement (PS_{Tape}), as illustrated in Fig. 1.

The statistical analysis presented in Table 5 indicates that there is a strong alignment between the manual and digital measurements. This is significant considering that field measurements typically have a recorded precision

Table 3 UAV system and on-board camera specifications

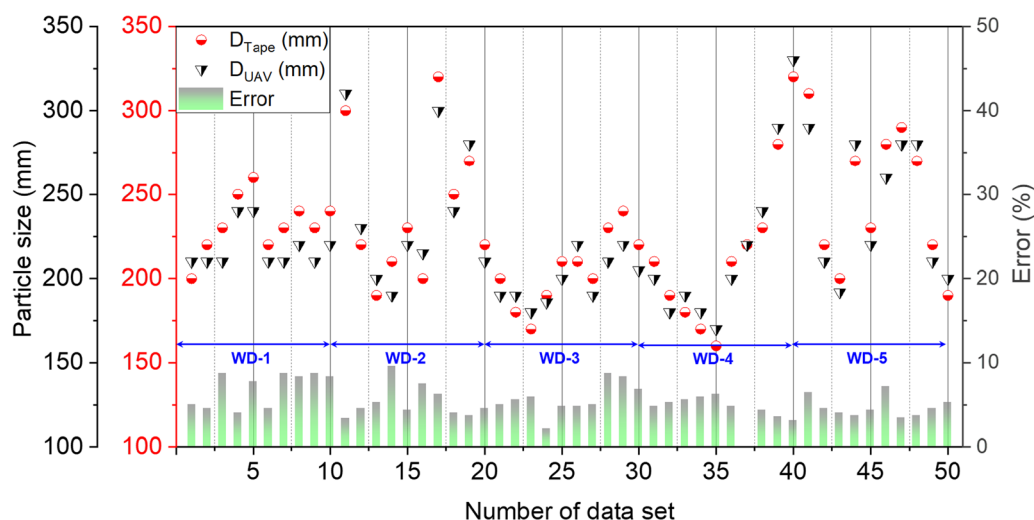| UAV system specifications					
UAV type	Weight	Diagonal size	Max. flight time	Satellite positioning	Gimbal stabilization
DJI Mavic Pro	735 g	335 mm	27 min	GPS/GLONASS	3-axis (pitch, roll, yaw)
On-board camera parameters					
Sensor	Lens	Frequency	Photograph IOS range	Image size	
1/2.3″ (CMOS). Pixels: 12 M	FOV 78.8° 26 mm	2.4 GHz	Video: 100–3200 Photo: 100–1600	4000 × 3000	

Fig. 5 Variation between digital analysis and field measurements across the five waste dumps

Table 5 Particle size distribution statistics for the five waste dumps: quartiles and extremes

Site	Number of datasets	Mean	Std.	Min.	Q1	Q2	Q3	Max.
WD-1	26	117.9	53.4	39.3	72.3	107.3	171.0	199.7
WD-2	32	88.6	65.7	43.1	61.1	68.2	73.1	395.9
WD-3	18	89.8	19.2	44.2	82.3	89.8	98.1	126.3
WD-4	7	770.6	35.6	724.0	749.6	763.1	791.0	825.9
WD-5	30	238.1	88.8	78.9	159.3	259.0	311.6	388.5

range of 50 to 100 mm [2]. The results affirm that UAV–SfM photogrammetry reliably quantifies particle size parameters with acceptable deviations. Figure 6 illustrates the error margin between field data and UAV photogrammetry, which is less than 10%, signifying a high correlation between actual data and digital analysis.

3.6 Defining shear strength model parameters.

3.6.1 PSD using UAV.

The application of the Structure-from-Motion (SfM) technique to the selected waste dumps generated point clouds ranging from 201,225 to 502,594 points [68]. Optimizing these point clouds involved aligning them with the ground control points (GCPs) field arrangement. This alignment helped minimize reprojection errors and enabled the creation of dense point clouds, consisting of approximately 190 million and 450 million points for all the sites, respectively. The drone data collection process entailed capturing multiple photographs to collect and accurately represent the geometric details of the rockfill and waste dump particles [31].

This study involved analyzing coarse materials from five different waste dumps and rockfill areas, with a focus on a wide range of gradations. A total of 3,855 images were taken, encompassing rockfill materials with particle sizes from sand and gravel to boulders as large as 1000 mm. These images were captured using a drone equipped with a GPS and an inertial navigation system, which allowed for recording the 3D spatial coordinates and the orientation of the camera. To ensure complete coverage of the areas, the drone was flown in four vertical paths, with each path overlapping the next, covering the entire targeted zones [10].

The photographs were captured from an average distance of 30 to 120 m from the surfaces of the waste dumps and rockfill slopes. This approach resulted in an estimated ground sample distance of approximately 1 cm. In this study, ShapeMetrix UAV software was employed to georeference the data, manage the point clouds, and quantify the particle size distribution (PSD) features [11]. Figure 7 illustrates the orientation of the photographs, while Fig. 5 presents the 3D model of waste dump WD-5.

Figure 8 displays the PSD analysis conducted using UAV imagery. In Fig. 9, the delineation of rockfill particles is shown using a rainbow scale, which facilitates the
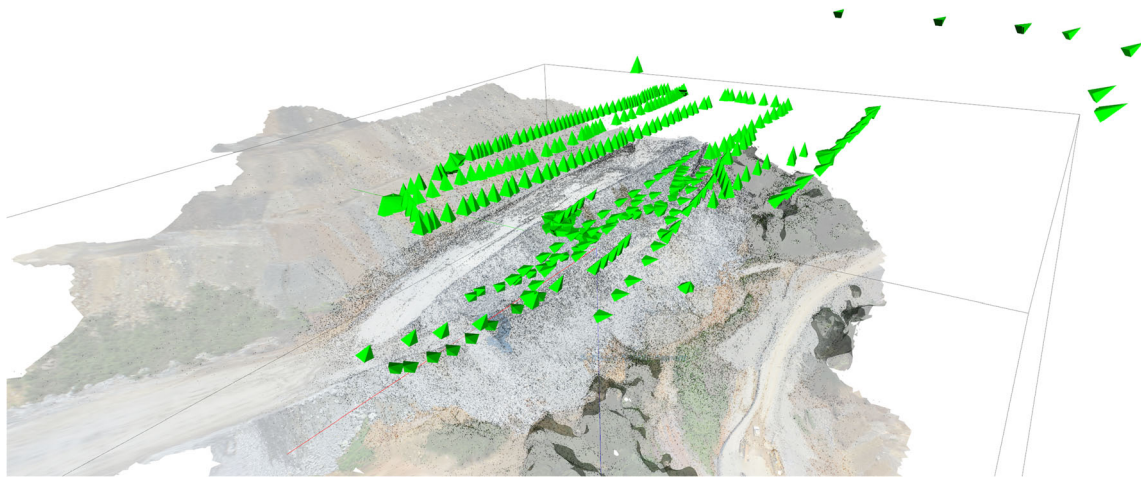
Fig. 6 Spatial arrangement and orientation of photographs in relation to the point cloud for waste dump WD-5
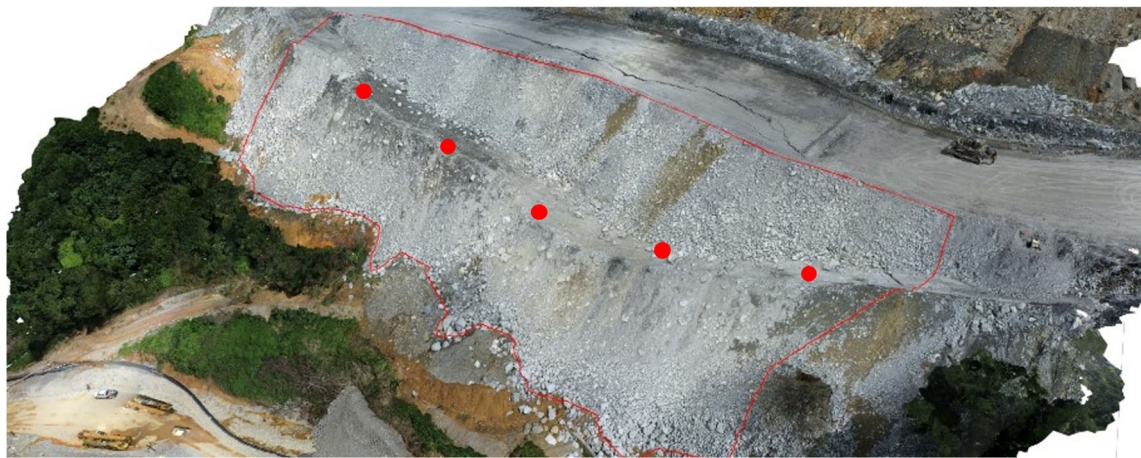

Fig. 7 3D model segment of waste dump WD-5, featuring over 7 million points and 2.6 million mesh elements. The model highlights the area encircled by the red line, with red dots indicating sampled boulder locations

Fig. 8 Detailed 3D model of waste dump WD-5, featuring over 7 million points and 2.6 million mesh elements

discretization of the 3D model for determining the average D50 of each area. The D50 value is a significant point on the PSD cumulative curve, representing the size below which 50% of the materials total volume in the sample is
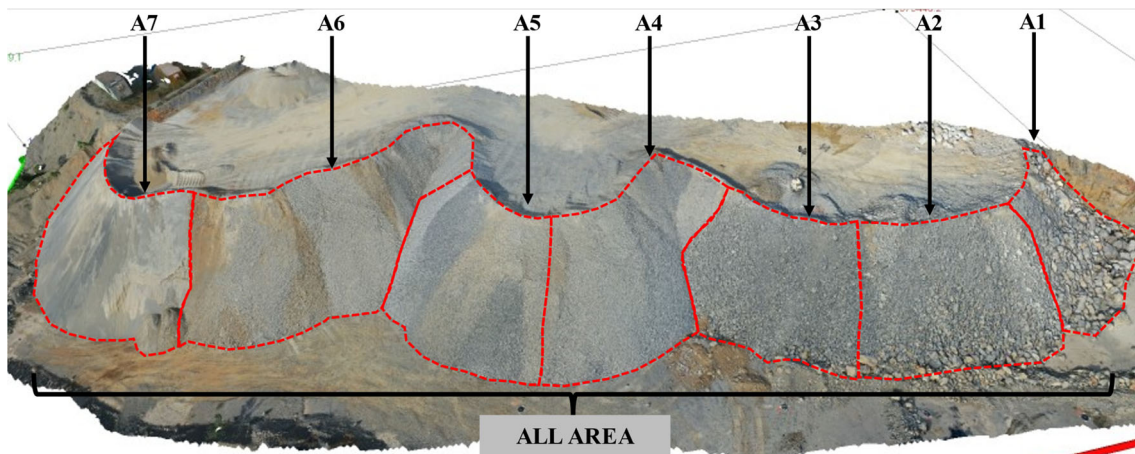
Fig. 9 Discretization example of the 3D model for WD-2, illustrating the process to determine the average D_{50} particle size in each area
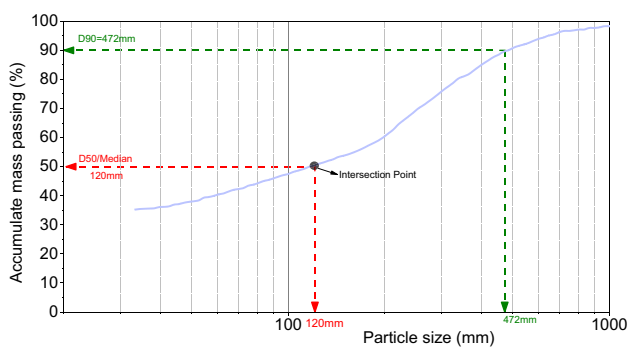
Fig. 10 Illustration of the D_{50} percentile derived from the PSD cumulative curve for waste dump WD-2

found. For instance, as illustrated in Fig. 10, a D_{50} of 120 mm indicates that half of the sample particles are 120 mm in size or smaller [19].

In the PSD cumulative curve shown in Fig. 10, the "x" axis displays particle sizes in millimeters on a log scale, and the "y" axis shows the cumulative percentage of smaller particles. To determine the D_{50}, which is the median particle size, a horizontal line is drawn at the 50% mark on the "y" axis. This line is extended to intersect the PSD curve. From this intersection, a vertical line is drawn downward to the "x" axis. In this specific case, the vertical line intersects the "x" axis at 120 mm, indicating the D_{50} value.

Figure 11 presents a discretized version of the 3D model, divided into several sections. This approach, as suggested in [61], is more user-friendly and easier to comprehend compared to the continuous values of D50. Such discretization typically results in smaller, more interpretable D_{50} values. Additionally, this method can enhance predictive accuracy for various diameters [38], including sizes ranging from boulders (larger than 1000 mm) to fines (smaller than 100 mm).

The PSD data obtained from the five waste dumps are presented in Fig. 12. By subdividing each area into smaller
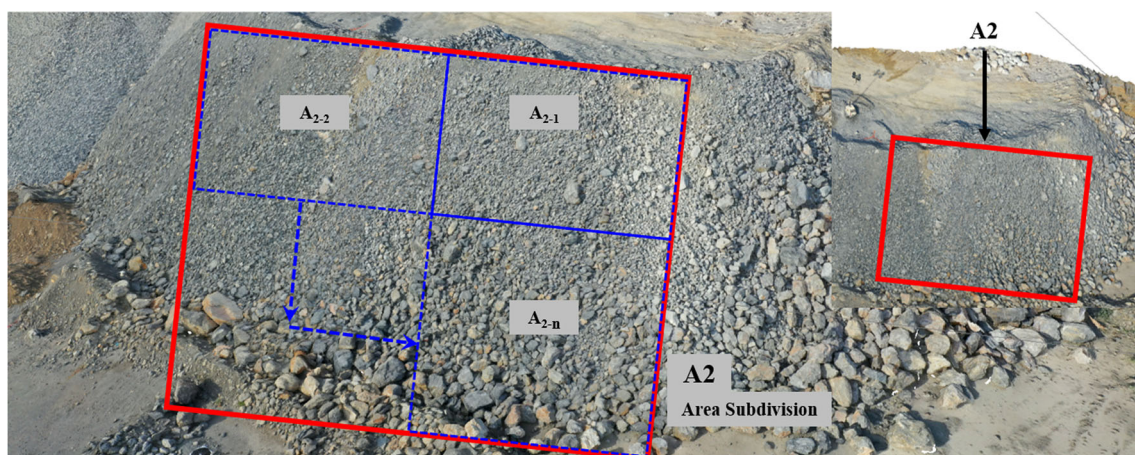

Fig. 11 Discretization of subareas in waste dump WD-2, with subarea A2 segmented into A2-2, A2-2, …A2-n, to analyse PSD variation through D_{50} subdivision
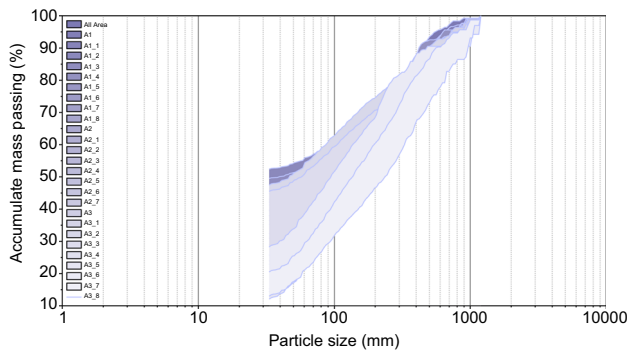
Fig. 12 Particle size distribution (PSD) and D_{50} values for subdivided subareas of waste dump WD-2
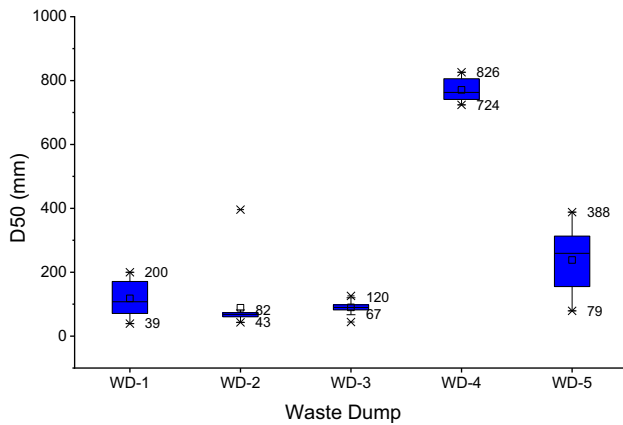

Fig. 13 Box–Whisker plot representing D_{50} values (in millimeters) across the five waste dumps

subareas, multiple D50 values for each waste dump are obtained. This approach, which leverages multiple data sources, enhances confidence in the model. Consequently, a substantial dataset of D50 values contributes to higher accuracy in the results.

To understand the influence of variability, appropriate values, and sensitivity, Table 5 and Fig. 13 illustrate different ranges of PSD and D_{50} values, considering the discretization process.
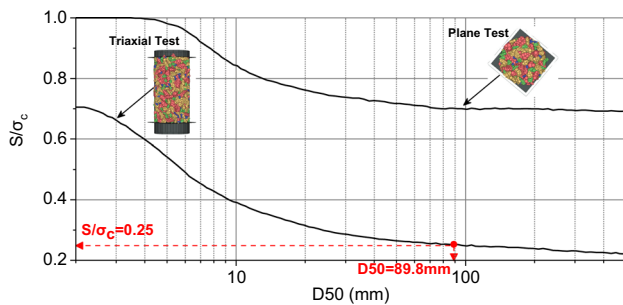
Fig. 14 Equivalent strength (S) for a D50 of 89.8 mm (modified [47])

3.7 *Equivalent strength (S/ σ_c).*

The equivalent strength, dependent on particle size, is calculated using the uniaxial compressive strength (UCS) of the parental rock and the D_{50}. This is based on the strength assessment method proposed by Barton and Kjaernsli [32], as shown in Fig. 14. For instance, the interpretation of the S value for a D50 of 89.8 mm is demonstrated using data from WD-3.

Table 6 presents the calculated equivalent particle strength values based on the mean D_{50} value for each waste dump. These values range from 0.20 for very coarse materials to 0.25 for medium materials (D50 < 100 mm). Mean values are employed to provide a singular, representative figure for estimating the equivalent particle strength. This approach is particularly useful given the multiple D_{50} values that can arise from the subdivision process. The primary goal of this study is to illustrate how equivalent strength values can be determined for a large dataset compiled using UAV for PSD estimation and shear strength calculation.

3.8 *Basic friction angle (φ_b).*

The basic friction angle (φ_b) is a crucial parameter in geotechnical analysis. It is typically estimated through tilting tests on dry, cut surfaces of the parent rock. In mining scenarios, φ_b is often derived from direct shear tests performed on cut samples from drill cores [13]. For this study, φ_b was calculated using multiple tilt tests. The results are presented in Table 7. Figure 15 illustrates the distribution of φ_b across each waste dump. Notably, in coarse materials like WD-2 (limestone), WD-4 (material with less than 15% fines), and WD-5 (rocky material), φ_b exhibits less variability, likely due to the lower fine content in these materials.

### 3.9 Dump porosity (n) and equivalent roughness of waste particles (R).

Waste rock volume typically experiences expansion during blasting, excavation, and dumping processes, covering a

Table 6 Equivalent particle strength for five waste dump sites using D_{50} means value

| Site	Mean	S/σ_c
WD-1	117.9	0.23
WD-2	88.6	0.25
WD-3	89.8	0.25
WD-4	770.6	0.20
WD-5	238.1	0.23

Table 7 Statistical data distribution on the basic friction angle (φ_b) from five waste dump sites

Site	Number of datasets	φ_b, Mean value	Std.	Min.	Q1	Q2	Q3	Max.
WD-1	20	26.9	1.6	25.0	26.0	26.5	28.0	30.0
WD-2	20	30.5	1.1	28.0	30.0	30.5	31.0	32.0
WD-3	20	26.9	1.5	25.0	26.0	26.5	28.0	29.0
WD-4	20	31.2	1.3	28.0	30.8	31.0	32.0	33.0
WD-5	20	31.3	1.1	30.0	30.0	31.0	32.0	33.0
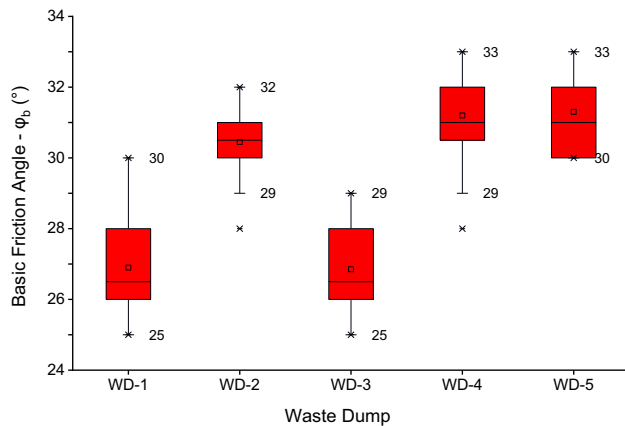
Fig. 15 Variation of basic friction angle (φ_b) across different waste dumps

broad range of particle sizes. This expansion is often quantified as a percentage increase from the undisturbed, in situ volume of the rock [50]. During the construction of dump faces, segregation is a common occurrence, and material consolidation under increased loading conditions tends to elevate the density while reducing both porosity and void ratio [21]. These dynamics pose challenges in accurately determining porosity, given the limited benchmark data available [85].

For this case study, conducting an in situ assessment of the dump density was not feasible. Consequently, a porosity value of 25% was assumed, derived from a thorough review of the literature and informed engineering judgment. The particle shape for all examined cases was conservatively estimated to have a smooth surface and moderate angle, with an assumed porosity of 25%. Utilizing the empirical method developed by Barton and Kjaernsli, as illustrated in Fig. 16, a roughness (R) value ranging between 6.0 and 6.5 was determined.
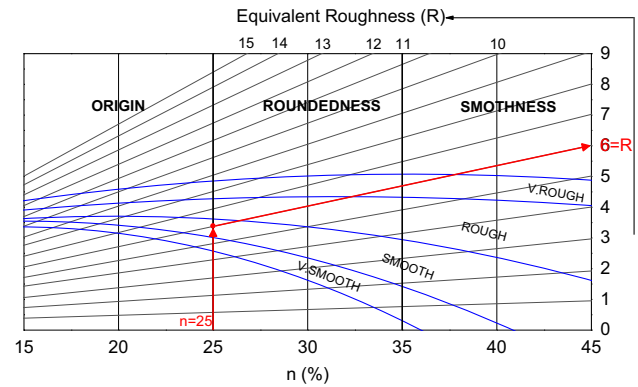
Fig. 16 Empirical derivation of equivalent R values (modified [47])

Table 8 Input parameters for the B–K nonlinear shear strength using normal stress of 1.0 MPa

Site	φ_b (°)	R	S/σ_c	σ_n (MPa)	τ (MPa)	φ' (°)
WD-1	26.9	6.1	0.23	1.0	0.67	33.87
WD-2	30.5	6.4	0.25	1.0	0.90	42.11
WD-3	26.9	6.0	0.25	1.0	0.71	35.27
WD-4	31.2	6.3	0.20	1.0	0.87	41.07
WD-5	31.3	6.5	0.23	1.0	0.94	43.25

3.10 Shear strength results using Barton–Kjaernsli criterion.

The key parameters referenced in Eq. (1) are detailed in Table 8. The shear strength was calculated using the B–K criterion, as outlined in Eq. (1), and was based on the mean values of φ_b (basic friction angle) and D_{50} [79].

Figure 17 and Fig. 18 present two groups of materials based on their shear response characteristics. The first group includes coarse materials with an UCS less than 20 MPa, while the second group consists of materials with a UCS greater than 30 MPa. This distinction may also relate to geological compositions. WD-1 and WD-3,
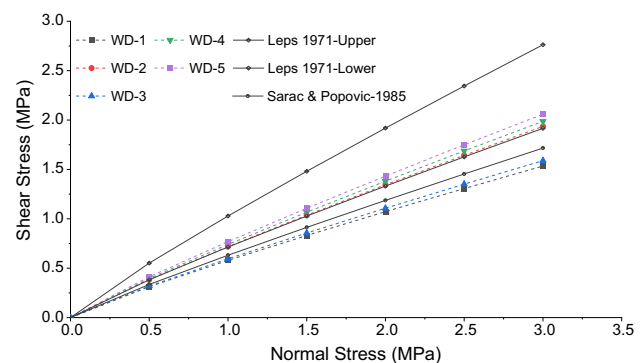
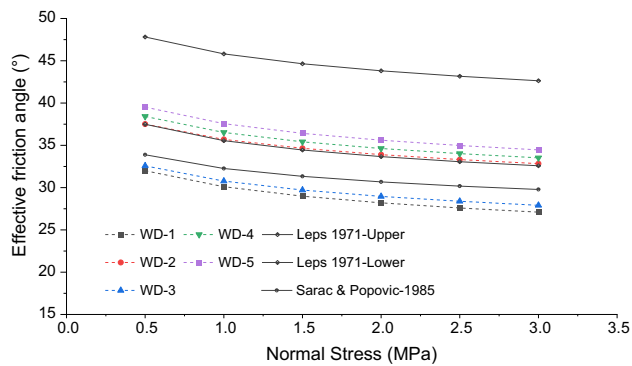**Fig. 17** Nonlinear shear strength envelopes using B–K criterion

Fig. 18 Effective friction angle using B–K criterion

primarily composed of carbonaceous-sediment mudstone with a high potential for acid generation and significant sulfide content, represent weaker materials. Conversely, rocky materials such as limestone (WD-2) and volcanic andesite (WD-4 and WD-5) are stronger, with higher UCS values. This suggests that coarser materials, associated with higher shear stresses, indicate more stable conditions [101].

To validate and compare this study findings, Fig. 17 and Fig. 18 also reference the seminal works of Leps [57] and Sarac and Popovic [89]. Leps research is widely acknowledged as a standard practice among geotechnical engineers in the mining sector, especially due to its endorsement as a guideline by the large open-pit (LOP) group [33]. This work is considered a standard reference for practical assessments. Notably, the data for WD-2, WD-4, and WD-5 are closely aligned with the lower bounds of Leps results. This alignment indicates that the B–K criterion is both applicable and consistent with established industry practices for stability assessments in hard rock and rocky materials.

Contrastingly, WD-1 and WD-3, characterized by their composition of carbonaceous-sediment mudstone with high acid generation potential and significant sulfide content, fall below Leps minimum shear envelope. This observation highlights a critical consideration when applying the B–K criterion to weaker materials, such as sedimentary rocks with lower UCS. In such cases, while the B–K criterion might underestimate the shear envelope, it can nonetheless provide a valuable starting point for preliminary feasibility assessments in scenarios where laboratory data are not available.

3.11 Sensitivity analysis of R and S in shear response using B–K criterion.

To fully comprehend the shear response, as illustrated in Fig. 17 and Fig. 18, and to address the limitations of this study, it is essential to analyze the impact of particle shape,

represented by R, and the strength of individual particles, denoted by S in the B–K criterion. This analysis will help determine whether segregation, particularly in high-end waste dumps, is predominantly influenced by particle size distribution (PSD) or by particle shape.

A key concept here involves understanding how shape and size polydispersity, which is the variation in particle size and shape irregularity, affect the strength properties of granular materials [4]. Studies on granular materials, especially those composed of pentagonal particles, indicate that while shear strength is not dependent on particle size, it does decrease with increased shape polydispersity [84].

This suggests that larger particles tend to bear stronger forces and are supported by a growing number of smaller particles. The observed independence of shear strength with respect to size variation is attributed to the self-organization of the contact network. This self-organization leads to a balance where the decrease in contact anisotropy is offset by an increase in force anisotropy [73].

Shear strength in granular materials is independent of particle size and is influenced by the shape and polydispersity of the particles. In consequence, as particle size decreases, cohesive forces become more pronounced relative to gravitational forces, impacting grain-to-grain interactions [3]. In consequence, properties such as grain shape and fragmentation susceptibility exhibit variation with particle size, emphasizing the significance of shape in the determination of shear strength [81].

Understanding the impact of superficial PSD estimation using UAV for shear strength characterization via the B–K criterion necessitates a sensitivity analysis, which is pivotal for identifying the limitations of this study. Analyzing the sensitivity of Eq. (1) involves examining how changes in roughness (R) and strength (S) influence shear strength (τ).

This examination is conducted by calculating the derivatives of τ with respect to R and S. Sensitivity is quantified as the derivative multiplied by the ratio of the parameter to the function value [91], a standard method in sensitivity analysis. Specifically, this is represented by $\frac{d\tau}{dR}\frac{R}{T}$ for R, with a similar approach for S. These calculations are essential for understanding how small variations in R and S affect the overall shear stress as defined by Eq. (1). The derivatives are expressed as follows:

Partial derivative of τ with respect to R:

$$d\tau/dR = \pi/180\sigma_{\mathrm{n}} \mathrm{Log}(S/\sigma_{\mathrm{n}}) \\ \times \left\{ \mathrm{Tan}^2[(R\,\mathrm{Log}(S/\sigma_{\mathrm{n}}) + \varphi_{\mathrm{b}})\pi/180 + 1] \right\} \tag{3}$$

This derivative assesses the sensitivity of τ to changes in R, considering the nonlinear influence of the tangent function and the logarithmic relationship.

Partial derivative of τ with respect to S:

$$d\tau/dS = \pi/180R\sigma_{\mathrm{n}}/S$$
$$\times \left\{ \mathrm{Tan}^2[(R\,\mathrm{Log}(S/\sigma_{\mathrm{n}}) + \varphi_{\mathrm{b}})\pi/180 + 1] \right\} \quad (4)$$

This derivative calculates how a small change in S impacts τ, considering the effects of the tangent function and the logarithmic relationship between S and σ_{n}.

Figure 19 demonstrates that the shear strength in WD-2, WD-4, and WD-5 is more sensitive to the shape of the particles [23] R than to the strength S. This observation aligns with the shear response illustrated in Fig. 17 and Fig. 18. On the contrary, the increased sensitivity to S in WD-1 and WD-3 can be attributed to their geological composition, which consists of carbonaceous-sediment mudstone. This material type, known for its high potential for acid generation and significant sulfide content, tends to be weaker.

The findings suggest that variations in particle shape, represented by R, have a considerable effect on final shear strength, particularly under higher normal stresses [76]. For engineering and design in rock mechanics, accurate assessment, integration of particle shape into models, and calculations are essential, as it significantly impacts the stability and safety of waste dump structures. This emphasizes a limitation in the B–K criterion application, especially for weak rocks and materials segregated during dumping sequences, often finer and located at the top crest of the sequence.

The lesser sensitivity to the scale factor S indicates that, while still important, its influence on shear strength relative to the applied normal stress is not as critical as the shape parameter R. However, this does not diminish S significance for weak materials like WD-1 and WD-3, where the sedimentary characteristics of the carbonaceous mudstone crucially affect the shear response, posing challenges in estimating particle shape and potentially leading to an oversight of this parameter, relying instead on the individual strength of the particles represented by S. This
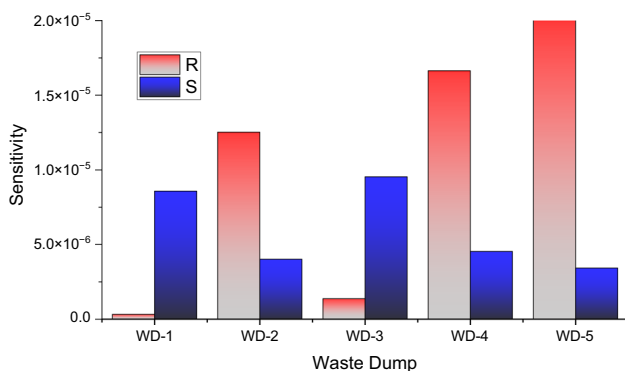

Fig. 19 Sensitivity analysis of R and S parameters for each waste dump

underlines that the effect of R is more pronounced within the considered range of normal stresses.

Finally, it is important to note that the actual sensitivity values and their implications can be highly site-specific, contingent on the unique geological conditions. While these observed trends offer general insights, site-specific analyses are paramount for precise and accurate rock mechanics assessments.

4 Conclusions

The following conclusions can be drawn from this study:

1. The percentage error for coarse characteristic size prediction ranges within $\pm 6\%$ when evaluated using UAV. With this quality of results, the determined PSD using photogrammetry saves the manual working time and reduces the bias due to segregation for full-scale waste dumps. Results show that for large-scale waste dumps when the reliability of the data is questionable with materials that contain "oversize" particles, UAV is shown to be a practical solution.

2. Results between field and digital measurements indicate that the average deviations and standard deviations between the manually measured and digitally determined particle size vary between 12.3 and 49.9 mm for field measurements and 16.9 and 52.5 mm for UAV with an average difference between the mean values of 4 mm. These well-matched results indicate that the UAV–SfM photogrammetry-based digital analysis can effectively identify and characterize the PSD for rockfills and waste dumps. Compared with the field measurements that are strongly restricted by measurement environments, the developed digital method is flexible, and the achieved results are reproducible.

3. The digital analysis can effectively identify particle size that may be neglected by the manual survey typically due to the limitations of surveying time and the harsh field environment and can be carried out at any concerned position with any scale and direction. The introduction and utilization of virtual waste dumps 3D models make it possible for quantitative PSD and extended material property analysis over large, unsafe, and inaccessible areas.

4. This study attempts to introduce the low-cost and lightweight UAV photogrammetry technique into the waste dump characterization, the development of which in future may become an important part in the next-generation field survey methods, and also provide a suitable tool for estimating shear strength for waste dumps and rockfill at large scale in active waste dumps basis.

Despite these promising results, the study acknowledges certain inherent limitations, which also serve as directions for future research:

1. Limited site access can restrict UAV data collection. Addressing this involves employing advanced UAV flight technologies and integrating UAV data with satellite imagery to cover extensive areas, even in restricted access sites.
2. The need for improved calibration methods is evident, especially for oversized particles. Enhancing calibration protocols and utilizing machine learning algorithms for calibration could lead to more accurate PSD estimations.
3. The limitation in data resolution can be mitigated by using higher-resolution cameras and more sensitive sensors. Combining UAV photogrammetry with other surveying techniques, like LiDAR, could create a more comprehensive dataset for PSD analysis.

The study highlights the need for continued research and technological advancements to fully leverage its capabilities in geotechnical applications. Addressing the identified limitations through advanced technologies and integrated methodologies will significantly enhance the effectiveness and applicability of UAV photogrammetry in environmental management and engineering.

References

1. Abellan A, Derron M-H, Jaboyedoff M (2016) Use of 3d point clouds in geohazards Special Issue: Current Challenges and Future Trends. Remote Sens (Basel). https://doi.org/10.3390/rs8020130
2. Akara MEM, Reeves DM, Parashar R (2020) Enhancing fracture-network characterization and discrete-fracture-network simulation with high-resolution surveys using unmanned aerial vehicles. Hydrogeol J 28:2285–2302. https://doi.org/10.1007/s10040-020-02178-y
3. Azéma E, Linero S, Estrada N, Lizcano A (2017) Shear strength and microstructure of polydisperse packings: The effect of size span and shape of particle size distribution. Phys Rev E 96:022902. https://doi.org/10.1103/PhysRevE.96.022902
4. Azéma E, Radjaï F, Peyroux R, Saussine G (2007) Force transmission in a packing of pentagonal particles. Phys Rev E 76:011301. https://doi.org/10.1103/PhysRevE.76.011301
5. Babaeian M, Ataei M, Sereshki F et al (2019) A new framework for evaluation of rock fragmentation in open pit mines. J Rock Mech Geotech Eng 11:325–336. https://doi.org/10.1016/J.JRMGE.2018.11.006
6. Bamford, Esmaeili, Schoellig A real-time analysis of rock fragmentation using UAV technology
7. Bamford T, Esmaeili K, Schoellig AP Aerial Rock Fragmentation Analysis in Low-Light Condition Using UAV Technology
8. Bamford T, Esmaeili K, Schoellig AP (2021) A deep learning approach for rock fragmentation analysis. Int J Rock Mech Min Sci 145:104839. https://doi.org/10.1016/J.IJRMMS.2021.104839
9. Bamford T, Medinac F, Esmaeili K (2020) Continuous monitoring and improvement of the blasting process in open pit mines using unmanned aerial vehicle techniques. Remote Sens (Basel) 12:2801. https://doi.org/10.3390/rs12172801
10. Bar N, Borgatti L, Donati D et al (2021) Classification of natural and engineered rock slopes using UAV photogrammetry for assessing stability. IOP Conf Ser Earth Environ Sci 833:012046. https://doi.org/10.1088/1755-1315/833/1/012046
11. Bar N, Kostadinovski M, Tucker M et al (2020) Rapid and robust slope failure appraisal using aerial photogrammetry and 3D slope stability models. Int J Min Sci Technol 30:651–658. https://doi.org/10.1016/J.IJMST.2020.05.013
12. Bar N, McQuillan A, Ma T et al (2023) A geotechnical evaluation of the CUMBA PIT SLOPE FAILURE, DOMINICAN REPUBLIC. IOP Conf Ser Earth Environ Sci 1124:012009. https://doi.org/10.1088/1755-1315/1124/1/012009
13. Barton N (2014) Non-linear Shear Strength for Rock, Rock Joints, Rockfill and Interfaces. In: Sexta conferencia Raul Marshal. Jalisco, Mexico
14. Barton N (2013) Shear strength criteria for rock, rock joints, rockfill and rock masses: problems and some solutions. J Rock Mech Geotech Eng 5:249–261. https://doi.org/10.1016/J.JRMGE.2013.05.008
15. Barton N (2016) Non-linear shear strength for rock, rock joints, rockfill and interfaces. Innov Infrastruct Solut 1:30. https://doi.org/10.1007/s41062-016-0011-1
16. Barton N, Kjærnsli B (1981) Shear strength of rockfill. J Geotech Eng Div 107:873–891. https://doi.org/10.1061/AJGEB6.0001167
17. Barton N, NR (2008) Shear Strength of Rockfill, Interfaces and Rock Joints, and their Points of Contact in Rock Dump Design. In: Proceedings of the First International Seminar on the Management of Rock Dumps, Stockpiles and Heap Leach Pads. Australian Centre for Geomechanics, Perth, pp 3–17
18. Bonilla-Rodríguez AJ, González LA, Walker JD, Santos H (2014) Strontium isotope (87Sr/86Sr) stratigraphy from the Coalcomana-Caprinuloidea rudist assemblage in the Greater Antilles (Puerto Rico, Dominican Republic and Jamaica). Cretac Res 50:97–109. https://doi.org/10.1016/J.CRETRES.2014.04.008
19. Boylu F, Dinçer H, Ateşok G (2004) Effect of coal particle size distribution, volume fraction and rank on the rheology of coal–water slurries. Fuel Process Technol 85:241–250. https://doi.org/10.1016/S0378-3820(03)00198-X
20. Breitenbach J (2012) Definition of rockfill versus earthfill material. J Indian Comm Larg Dams 1:8–12

21. Brown AJ (1988) Use of soft rockfill at Evretou Dam, Cyprus. Géotechnique 38:333–354. https://doi.org/10.1680/geot.1988.38.3.333

22. Bujak B, Bottlinger M (2008) Three-dimensional measurement of particle shape. Part Part Syst Charact 25:293–297. https://doi.org/10.1002/ppsc.200800027

23. Cantor D, Azéma E, Preechawuttipong I (2020) Microstructural analysis of sheared polydisperse polyhedral grains. Phys Rev E 101:062901. https://doi.org/10.1103/PhysRevE.101.062901

24. Cardona J, Ferreira C, McGinty J et al (2018) Image analysis framework with focus evaluation for in situ characterisation of particle size and shape attributes. Chem Eng Sci 191:208–231. https://doi.org/10.1016/J.CES.2018.06.067

25. Carrasco S, Cantor D, Ovalle C (2022) Effects of particle size-shape correlations on steady shear strength of granular materials: the case of particle elongation. Int J Numer Anal Methods Geomech 46:979–1000. https://doi.org/10.1002/nag.3329

26. Casali A, Gonzalez G, Vallebuona G et al (2001) Grindability soft-sensors based on lithological composition and on-line measurements. Miner Eng 14:689–700. https://doi.org/10.1016/S0892-6875(01)00065-6

27. Charles JA (1991) Laboratory Shear Strength Tests and the Stability of Rockfill Slopes. In: das Neves EM (ed) Advances in Rockfill Structures. Springer Netherlands, Dordrecht, pp 53–72

28. Charles JA, Watts KS (1980) The influence of confining pressure on the shear strength of compacted rockfill. Géotechnique 30:353–367. https://doi.org/10.1680/geot.1980.30.4.353

29. Chen Q, Li Z, Dai Z et al (2023) Mechanical behavior and particle crushing of irregular granular material under high pressure using discrete element method. Sci Rep 13:7843. https://doi.org/10.1038/s41598-023-35022-w

30. Cobian J, Bautista M, Bar N, Hammah R (2022) 3D Limit Equilibrium Analysis and Risk Appraisal of Hondo Waste Rock Stockpile Designs. In: Rocscience Africa Conference 2022. Accra

31. Colomina I, Molina P (2014) Unmanned aerial systems for photogrammetry and remote sensing: a review. ISPRS J Photogramm Remote Sens 92:79–97. https://doi.org/10.1016/J.ISPRSJPRS.2014.02.013

32. Contreras L-F, Linero-Molina S, Dixon J (2022) Bayesian Approach To Improve The Confidence Of The Estimation Of The Shear Strength Of Coarse Mine Waste Using Barton's Empirical Criterion. Australian Geomechanics Journal. https://doi.org/10.56295/AGJ5728

33. Cunning J, Hawley M (2017) Guidelines for Mine Waste Dump and Stockpile Design. CSIRO, pp 79–98

34. Da-Mang L (1992) Angles of friction of granular fills. University of Cambridge

35. Dano C, Ovalle C, Yin ZY et al (2018) Behavior of granular materials affected by grain breakage. Adv Multi-Phy Multi-Scale Couplings Geo-Environ Mech. https://doi.org/10.1016/B978-1-78548-278-6.50004-9

36. Deiminiat A, Li L (2022) Experimental study on the reliability of scaling down techniques used in direct shear tests to determine the shear strength of rockfill and waste rocks. CivilEng 3:35–50. https://doi.org/10.3390/civileng3010003

37. Deiminiat A, Li L, Zeng F et al (2020) Determination of the shear strength of rockfill from small-scale laboratory shear tests: a critical review. Adv Civil Eng 2020:1–18. https://doi.org/10.1155/2020/8890237

38. Domingos P, Pazzani M (1997) On the optimality of the simple bayesian classifier under zero-one loss. Mach Learn 29:103–130. https://doi.org/10.1023/A:1007413511361

39. Dorador L, Villalobos FA (2020) Analysis of the geomechanical characterization of coarse granular materials using the parallel gradation method. Obras y proyectos. https://doi.org/10.4067/S0718-28132020000100050

40. Doruk P (1991) Analysis of the laboratory strength data using the original and modified Hoek-Brown failure criteria. University of Toronto

41. Frossard E, Hu W, Dano C, HICHER P-Y, (2012) Rockfill shear strength evaluation: a rational method based on size effects. Géotechnique 62:415–427. https://doi.org/10.1680/geot.10.P.079

42. Gaich A, Pötsch M (2022) Automatic 3D fragmentation analysis from drone imagery. In: 48th Annual Conference on Explosives and Blasting. Las Vegas

43. Gallagher E (1976) Optoelectronic Coarse Particle Size Analysers for Industrial Measurement. University of Queensland

44. Gao S, Zhou W, Shi X et al (2017) Mechanical properties of material in a mine dump at the Shengli #1 Surface Coal Mine, China. Int J Min Sci Technol 27:545–550. https://doi.org/10.1016/J.IJMST.2017.03.014

45. Gonzalez Garcia A (1985) Rockfill strength with dimensionless parameters. In: Proceedings of the Eleventh International Conference on Soil Mechanics and Foundation Engineering. San Francisco, pp 479–485

46. Hamzeloo E, Massinaei M, Mehrshad N (2014) Estimation of particle size distribution on an industrial conveyor belt using image analysis and neural networks. Powder Technol 261:185–190. https://doi.org/10.1016/J.POWTEC.2014.04.038

47. Hyslip JP, Vallejo LE (1997) Fractal analysis of the roughness and size distribution of granular materials. Eng Geol 48:231–244. https://doi.org/10.1016/S0013-7952(97)00046-X

48. Indraratna B (1994) The effect of normal stress-friction angle relationship on the stability analysis of a rockfill dam. Geotech Geol Eng 12:113–121. https://doi.org/10.1007/BF00429769

49. Indraratna B, Ionescu D, Christie HD (1998) Shear behavior of railway ballast based on large-scale triaxial tests. J Geotech Geoenviron Eng 124:439–449. https://doi.org/10.1061/(ASCE)1090-0241(1998)124:5(439)

50. Indraratna B, Wijewardena LSS, Balasubramaniam AS (1993) Large-scale triaxial testing of grey wacke rockfill. Géotechnique 43:37–51. https://doi.org/10.1680/geot.1993.43.1.37

51. Jang H, Kitahara I, Kawamura Y et al (2020) Development of 3D rock fragmentation measurement system using photogrammetry. Int J Min Reclam Environ 34:294–305. https://doi.org/10.1080/17480930.2019.1585597

52. Kaunda R (2015) Predicting shear strengths of mine waste rock dumps and rock fill dams using artificial neural networks. Int J Min Miner Eng 6:139–171. https://doi.org/10.1504/IJMME.2015.070378

53. Kemeny J (1994) Practical technique for determining the size distribution of blasted benches, waste dumps and heap leach sites. Min Eng 46:1281–1284

54. Koizomi F, Kunugita E, Nishitani H (1994) Image Processing for Quality/Process Control of Polymer Process. In: Proceedings of Process Systems Engineering

55. Kong D, Saroglou C, Wu F et al (2021) Development and application of UAV-SfM photogrammetry for quantitative characterization of rock mass discontinuities. Int J Rock Mech Min Sci 141:104729. https://doi.org/10.1016/j.ijrmms.2021.104729

56. Latham J-P, Kemeny J, Maerz N et al (2003) A blind comparison between results of four image analysis systems using a photo-library of piles of sieved fragments. Fragblast 7:105–132. https://doi.org/10.1076/frag.7.2.105.15899

57. Leps TM (1970) Review of shearing strength of rockfill. J Soil Mech Found Division 96:1159–1170. https://doi.org/10.1061/JSFEAQ.0001433

58. Li G, Liu Y-J, Dano C, Hicher P-Y (2015) Grading-dependent behavior of granular materials: from discrete to continuous modeling. J Eng Mech. https://doi.org/10.1061/(ASCE)EM.1943-7889.0000866

59. Lin CL, Miller JD (1993) The development of a PC, image-based, on-line particle-size analyzer. Min Metall Explor 10:29–35. https://doi.org/10.1007/BF03402996

60. Linero Molina S, Contreras LF, Dixon J (2021) Estimation of shear strength of very coarse mine waste. In: SSIM 2021: Second International Slope Stability in Mining. Australian Centre for Geomechanics, Perth, pp 341–354

61. Liu H, Hussain F, Tan CL, Dash M (2002) Discretization: an enabling technique. Data Min Knowl Discov 6:393–423. https://doi.org/10.1023/A:1016304305535

62. Lu F, Zhou X, He Y (1988) Image segmentation technique used in estimation of the size distribution of rock fragments in mining. In: Proceedings of IAPR Workshop on Computer Vision - Special Hardware and Industrial Applications, MVA 1988, Tokyo, Japan, October 12–14, 1988. pp 351–354

63. Marsal RJ (1967) Large scale testing of rockfill materials. J Soil Mech Found Division 93:27–43. https://doi.org/10.1061/JSFEAQ.0000958

64. Marschi ND, Chan CK, Seed HB (1972) Evaluation of properties of rockfill materials. J Soil Mech Found Division 98:95–114. https://doi.org/10.1061/JSFEAQ.0001735

65. Marshal R (1973) Mechanical properties of rockfill. Embankment Dam Engineering, pp 109–200

66. Mattson PH (1979) Subduction, buoyant braking, flipping, and strike-slip faulting in the northern caribbean. J Geol 87:293–304. https://doi.org/10.1086/628418

67. De Mello VFB (1977) Reflections on design decisions of practical significance to embankment dams. Géotechnique 27:281–355. https://doi.org/10.1680/geot.1977.27.3.281

68. Mineo S, Caliò D, Pappalardo G (2022) UAV-based photogrammetry and infrared thermography applied to rock mass survey for geomechanical purposes. Remote Sens (Basel) 14:473. https://doi.org/10.3390/rs14030473

69. Miura S, Yagi K, Asonuma T (2003) Deformation-strength evaluation of crushable volcanic soils by laboratory and in-situ testing. Soils Found 43:47–57. https://doi.org/10.3208/SANDF.43.4_47

70. Nakata AFL, Hyde M, Hyodo H, Murata, (1999) A probabilistic approach to sand particle crushing in the triaxial test. Géotechnique 49:567–583. https://doi.org/10.1680/geot.1999.49.5.567

71. Nelson CE (2000) Volcanic domes and gold mineralization in the Pueblo Viejo district, Dominican Republic. Miner Depos 35:511–525. https://doi.org/10.1007/s001260050258

72. Newland PL, Allely BH (1957) Volume changes in drained taixial tests on granular materials. Géotechnique 7:17–34. https://doi.org/10.1680/geot.1957.7.1.17

73. Nguyen D-H, Azéma E, Sornay P, Radjai F (2015) Effects of shape and size polydispersity on strength properties of granular materials. Phys Rev E 91:032203. https://doi.org/10.1103/PhysRevE.91.032203

74. Nick B, Bjørn K (1981) Shear strength of rockfill. J Geotech Eng Div 107:873–891. https://doi.org/10.1061/AJGEB6.0001167

75. Ord A (1988) Real-time image analysis of size and shape distributions of rock fragments. In: The AusIMM. pp 115–119

76. Ovalle C, Dano C (2020) Effects of particle size–strength and size–shape correlations on parallel grading scaling. Géotech Lett 10:191–197. https://doi.org/10.1680/jgele.19.00095

77. Ovalle C, Frossard E, Dano C et al (2014) The effect of size on the strength of coarse rock aggregates and large rockfill samples through experimental data. Acta Mech 225:2199–2216. https://doi.org/10.1007/s00707-014-1127-z

78. Ovalle C, Linero S, Dano C et al (2020) Data compilation from large drained compression triaxial tests on coarse crushable rockfill materials. J Geotech Geoenviron Eng. https://doi.org/10.1061/(ASCE)GT.1943-5606.0002314

79. Oyanguren PR, Nicieza CG, Fernández MIÁ, Palacio CG (2008) Stability analysis of Llerin Rockfill Dam: An in situ direct shear test. Eng Geol 100:120–130. https://doi.org/10.1016/J.ENGGEO.2008.02.009

80. Özyeşil O, Voroninski V, Basri R, Singer A (2017) A survey of structure from motion. Acta Numer 26:305–364. https://doi.org/10.1017/S096249291700006X

81. Parteli EJR, Schmidt J, Blümel C et al (2014) Attractive particle interaction forces and packing density of fine glass powders. Sci Rep 4:6227. https://doi.org/10.1038/srep06227

82. Pindell JL (1991) Geologic rationale for hydrocarbon exploration in the caribbean and adjacent regions. J Pet Geol 14:237–258. https://doi.org/10.1111/j.1747-5457.1991.tb00310.x

83. Qiu P, Pabst T (2023) Characterization of particle size segregation and heterogeneity along the slopes of a waste rock pile using image analysis. Environ Earth Sci 82:573. https://doi.org/10.1007/s12665-023-11229-y

84. Rothenburg L, Bathurst RJ (1989) Analytical study of induced anisotropy in idealized granular materials. Géotechnique 39:601–614. https://doi.org/10.1680/geot.1989.39.4.601

85. Rowe PW (1991) A reassessment of the causes of the Carsington embankment failure. Géotechnique 41:395–421. https://doi.org/10.1680/geot.1991.41.3.395

86. Saadoun A, Fredj M, Boukarm R, Hadji R (2022) Fragmentation analysis using digital image processing and empirical model (KuzRam): a comparative study. Journal of Mining Institute Online first. https://doi.org/10.31897/PMI.2022.84

87. Sanchidrián JA, Segarra P, López LM (2006) A practical procedure for the measurement of fragmentation by blasting by image analysis. Rock Mech Rock Eng 39:359–382. https://doi.org/10.1007/s00603-005-0073-4

88. Sanchidrián JA, Segarra P, Ouchterlony F, López LM (2009) On the accuracy of fragment size measurement by image analysis in combination with some distribution functions. Rock Mech Rock Eng 42:95–116. https://doi.org/10.1007/s00603-007-0161-8

89. Sarac D, Popovic M (1985) Shear strength of rockfill and slope stability. In: Proceedings of the Eleventh International Conference on Soil Mechanics and Foundation Engineering. San Francisco, pp 641–645

90. Shin H, Santamarina JC (2013) Role of particle angularity on the mechanical behavior of granular mixtures. J Geotech Geoenviron Eng 139:353–355. https://doi.org/10.1061/(ASCE)GT.1943-5606.0000768

91. Smith ED, Szidarovszky F, Karnavas WJ, Bahill AT (2007) Sensitivity analysis, a powerful system validation technique. Open Cybern Syst J 2:39–56. https://doi.org/10.2174/1874110X00802010039

92. Stauder S, Buyer A (2018) Advances in the Development of a Novel Algorithm for Fragmentation Analysis Based on Photogrammetry

93. Thurley MJ (2013) Automated Image Segmentation and Analysis of Rock Piles in an Open-Pit Mine. In: 2013 International Conference on Digital Image Computing: Techniques and Applications (DICTA). pp 1–8

94. Thurley MJ (2002) Three dimensional data analysis for the separation and sizing of rock piles in mining

95. Thurley MJ (2009) Automated online measurement of particle size distribution using 3D range data. IFAC Proceedings Volumes 42:134–139. https://doi.org/10.3182/20091014-3-CL-4011.00025

96. Torró L, Proenza JA, Aiglsperger T et al (2017) Geological, geochemical and mineralogical characteristics of REE-bearing Las Mercedes bauxite deposit, Dominican Republic. Ore Geol Rev 89:114–131. https://doi.org/10.1016/J.OREGEOREV.2017.06.017

97. Valenzuela L, Bard E, Campana J, Anabalon M (2008) High waste rock dumps — challenges and developments. In: Proceedings of the First International Seminar on the Management of Rock Dumps, Stockpiles and Heap Leach Pads. Australian Centre for Geomechanics, Perth, pp 65–78

98. Vallerga B, Seed H, Monismith C, Cooper R (1957) Effect of Shape, Size, and Surface Roughness of Aggregate Particles on the Strength of Granular Materials. In: Road and Paving Materials. ASTM International, 100 Barr Harbor Drive, PO Box C700, West Conshohocken, PA 19428–2959, pp 63–63–14

99. Westoby MJ, Brasington J, Glasser NF et al (2012) 'Structure-from-Motion' photogrammetry: A low-cost, effective tool for geoscience applications. Geomorphology 179:300–314. https://doi.org/10.1016/J.GEOMORPH.2012.08.021

100. Wu X, Kemeny JM (1992) A segmentation method for multi-connected particle delineation. [1992] Proceedings IEEE Workshop on Applications of Computer Vision. IEEE Comput. Soc. Press, USA, pp 240–247

101. Wu ZY, Li YL, Chen JK et al (2013) A reliability-based approach to evaluating the stability of high rockfill dams using a nonlinear shear strength criterion. Comput Geotech 51:42–49. https://doi.org/10.1016/J.COMPGEO.2013.01.005

102. Xu Y (2018) Fractal dimension of demolition waste fragmentation and its implication of compactness. Powder Technol 339:922–929. https://doi.org/10.1016/J.POWTEC.2018.08.071

103. Xu Y, Feng X, Zhu H, Chu F (2015) Fractal model for rockfill shear strength based on particle fragmentation. Granul Matter 17:753–761. https://doi.org/10.1007/s10035-015-0591-z

104. Yaghoobi H, Mansouri H, Ebrahimi Farsangi MA, Nezamabadi-Pour H (2019) Determining the fragmented rock size distribution using textural feature extraction of images. Powder Technol 342:630–641. https://doi.org/10.1016/J.POWTEC.2018.10.006

105. Yan WM, Dong J (2011) Effect of particle grading on the response of an idealized granular assemblage. Int J Geomech 11:276–285. https://doi.org/10.1061/(ASCE)GM.1943-5622.0000085

106. Yang G, Jiang Y, Nimbalkar S et al (2019) Influence of particle size distribution on the critical state of rockfill. Adv Civil Eng 2019:1–7. https://doi.org/10.1155/2019/8963971

107. Yen YK, Lin CL, Miller JD (1998) Particle overlap and segregation problems in on-line coarse particle size measurement. Powder Technol 98:1–12. https://doi.org/10.1016/S0032-5910(97)03405-0

108. Zekkos D, Professor A, Greenwood W, et al Lessons Learned from the Application of UAV-Enabled Structure-From-Motion Photogrammetry in Geotechnical Engineering. International Journal of Geoengineering Case Histories © 4:254. https://doi.org/10.4417/IJGCH-04-04-03

109. Zerui L, Behrooz GN, Mahdi MD (2017) An Innovative Approach to Determine Particle Size Distribution for Rockfill Material.In: International Journal Of Rock Mechanics And Mining Sciences 26–35

110. Zhang Z, Yang J, Ding L, Zhao Y (2012) Estimation of coal particle size distribution by image segmentation. Int J Min Sci Technol 22:739–744. https://doi.org/10.1016/J.IJMST.2012.08.026